**EJNMMI Research**
a SpringerOpen Journal

**ORIGINAL RESEARCH**                                    **Open Access**

# A comparison of $^{111}$In- or $^{64}$Cu-DOTA-trastuzumab Fab fragments for imaging subcutaneous HER2-positive tumor xenografts in athymic mice using microSPECT/CT or microPET/CT

Conrad Chan[1], Deborah A Scollard[1], Kristin McLarty[1], Serena Smith[1] and Raymond M Reilly[1,2,3*]

## Abstract

**Background:** Our objective was to compare $^{111}$In- or $^{64}$Cu-DOTA-trastuzumab Fab fragments for imaging small or large s.c. tumor xenografts in athymic mice that display a wide range of human epidermal growth factor receptor-2 (HER2) expression using microSPECT/CT or microPET/CT.

**Methods:** Trastuzumab Fab were labeled with $^{111}$In or $^{64}$Cu by conjugation to 1,4,7,10-tetraazacyclododecane N, N', N'', N'''-tetraacetic acid (DOTA). The purity of $^{111}$In- and $^{64}$Cu-DOTA-trastuzumab Fab was measured by SDS-PAGE and HPLC. HER2 binding affinity was determined in saturation radioligand binding assays using SKBR-3 cells ($1.3 \times 10^6$ HER2/cell). MicroSPECT/CT and microPET/CT were performed in athymic mice bearing s.c. BT-20 and MDA-MB-231 xenografts with low (0.5 to $1.6 \times 10^5$ receptors/cell), MDA-MB-361 tumors with intermediate ($5.1 \times 10^5$ receptors/cell) or SKOV-3 xenografts with high HER2 expression ($1.2 \times 10^6$ receptors/cell) at 24 h p.i. of 70 MBq (10 µg) of $^{111}$In-DOTA-trastuzumab Fab or 22 MBq (10 µg) of $^{64}$Cu-DOTA-trastuzumab Fab or irrelevant $^{111}$In- or $^{64}$Cu-DOTA-rituximab Fab. Tumor and normal tissue uptake were quantified in biodistribution studies.

**Results:** $^{111}$In- and $^{64}$Cu-DOTA-trastuzumab were > 98% radiochemically pure and bound HER2 with high affinity ($K_d = 20.4 \pm 2.5$ nM and $40.8 \pm 3.5$ nM, respectively). MDA-MB-361 and SKOV-3 tumors were most clearly imaged using $^{111}$In- and $^{64}$Cu-DOTA-trastuzumab Fab. Significantly higher tumor/blood ($T/B$) ratios were found for $^{111}$In-DOTA-trastuzumab Fab than $^{111}$In-DOTA-rituximab Fab for BT-20, MDA-MB-231 and MDA-MB-361 xenografts, and there was a direct association between $T/B$ ratios and HER2 expression. In contrast, tumor uptake of $^{64}$Cu-DOTA-trastuzumab Fab was significantly higher than $^{64}$Cu-DOTA-rituximab Fab in MDA-MB-361 tumors but no direct association with HER2 expression was found. Both $^{111}$In- and $^{64}$Cu-DOTA-trastuzumab Fab imaged small (5 to 10 mm) or larger (10 to 15 mm) MDA-MB-361 tumors. Higher blood, liver, and spleen radioactivity were observed for $^{64}$Cu-DOTA-trastuzumab Fab than $^{111}$In-DOTA-trastuzumab Fab.

**Conclusions:** We conclude that $^{111}$In-DOTA-trastuzumab Fab was more specific than $^{64}$Cu-DOTA-trastuzumab Fab for imaging HER2-positive tumors, especially those with low receptor density. This was due to higher levels of circulating radioactivity for $^{64}$Cu-DOTA-trastuzumab Fab which disrupted the relationship between HER2 density and $T/B$ ratios. Use of alternative chelators that more stably bind $^{64}$Cu may improve the association between $T/B$ ratios and HER2 density for $^{64}$Cu-labeled trastuzumab Fab.

**Keywords:** indium-111, copper-64, HER2, MicroSPECT, MicroPET, DOTA, trastuzumab Fab, breast cancer, ovarian cancer

\* Correspondence: raymond.reilly@utoronto.ca
[1]Department of Pharmaceutical Sciences, University of Toronto, Toronto, M5S 3M2, ON, Canada
Full list of author information is available at the end of the article

Springer

# Background

The human epidermal growth factor receptor-2 (HER2) is overexpressed in 20% to 25% of breast cancers (BC) and is the target for treatment with trastuzumab (Herceptin), a humanized IgG$_1$ monoclonal antibody (mAb) [1,2]. HER2 amplification is normally assessed *ex vivo* in a primary tumor biopsy by immunohistochemical (IHC) staining for HER2 protein or by fluorescence *in situ* hybridization to detect increased *HER2* gene copy number [3]. However, discordance in HER2 expression between primary and metastatic BC has been found in 20% to 30% of cases [4,5] and thus, it would be useful to have an imaging technique to assess HER2 phenotype *in situ* in BC lesions. Several investigators have shown that HER2 expression can be imaged in human BC xenografts in athymic mice by single photon emission computed tomography (SPECT) using trastuzumab or its Fab fragments labeled with ^{111}In or [99m]Tc [6-9]. These studies have been extended to imaging HER2-positive BC in patients using ^{111}In-labeled trastuzumab IgG [2,10]. More recently, positron-emission tomography (PET) using trastuzumab labeled with [89]Zr has shown promise for imaging HER2 expression in tumor xenograft mouse models and in patients with metastatic BC [11,12]. Imaging also offers an opportunity to detect response to HER2-targeted therapies in BC [13]. We previously reported that SPECT with ^{111}In-labeled pertuzumab (anti-HER2) detected early response to treatment with trastuzumab (Herceptin) in athymic mice bearing s.c. MDA-MB-361 BC xenografts [14]. Smith-Jones et al. demonstrated that PET with ^{68}Ga-labeled trastuzumab F(ab')$_2$ fragments identified response of HER2-positive BT-474 human BC tumors in mice to treatment with heat shock protein (Hsp90) inhibitors [15].

PET offers several potential advantages compared to SPECT for imaging tumors because it has higher intrinsic sensitivity, is more easily quantified, and in some instances offers higher spatial resolution. Despite these apparent benefits, few studies have reported a comparison of PET and SPECT for imaging HER2-positive tumors using the same agent labeled with a single photon-emitter or positron-emitter. Dijkers et al. compared [89]Zr- and ^{111}In-labeled trastuzumab in mice bearing s.c. SK-OV-3 human ovarian cancer xenografts and reported no significant differences in tumor and normal tissue uptake [12]. MicroPET with [89]Zr-labeled trastuzumab visualized these tumors, but the corresponding microSPECT images with ^{111}In-labeled trastuzumab were not presented.

In this study, we compared microSPECT/CT and microPET/CT for imaging s.c. human tumor xenografts expressing a wide range of HER2 density in athymic mice using trastuzumab Fab fragments modified with 1,4,7,10-tetraazacyclododecane N, N', N'', N'''-tetraacetic acid (DOTA) for complexing ^{111}In or [64]Cu. [64]Cu decays

with a half-life of 12.7 h by positron emission [E$\beta^+$ = 0.65 MeV (17.4%)], $\beta^-$ emission [E$\beta$ = 0.58 MeV (39%)] and electron capture (43.6%). [111]In decays by electron capture with a half-life of 2.8 days emitting Auger electrons and two γ-photons [E$\gamma$ = 171 keV (90%) and 245 keV (94%)]. DOTA was selected as a chelator because both ^{111}In and ^{64}Cu form thermodynamically stable complexes with DOTA (K$_d$ = $10^{24}$ and $10^{23}$ M$^{-1}$, respectively) [16,17]. [64]Cu complexed to DOTA and linked to mAbs and peptides has been widely studied for PET imaging of tumors [15,18-23]. Fab fragments were selected for these studies because their pharmacokinetics of tumor uptake and elimination from the blood and normal tissues is compatible with the half-lives of ^{64}Cu and [111]In [24].

# Materials and methods

## Preparation of Fab fragments

Trastuzumab (Herceptin) and rituximab (anti-CD20; Rituxan) are humanized IgG$_1$ mAbs and were obtained from Roche Pharmaceuticals Ltd. (Mississauga, ON, Canada). Fab fragments were prepared by digestion with immobilized papain (Pierce Chemical Co., Rockford, IL, USA) and purified as reported [7,25]. Fab purity was assessed by sodium dodecyl sulfate polyacrylamide gel electrophoresis (SDS-PAGE) on a 4% to 20% Tris HCl gradient mini-gel (BioRad, Mississauga, ON, Canada) and by size-exclusion high performance liquid chromatography (HPLC). For SDS-PAGE, Fab (10 μg) were electrophoresed under non-reducing and reducing [dithiothreitol (DTT)] conditions. The gel was stained with Coomassie R-250 brilliant blue (Bio-Rad). Size-exclusion HPLC was performed on a BioSep SEC-2000 column (Phenomenex, Torrance, CA, USA) eluted with 100 mM NaH$_2$PO$_4$ buffer (pH 7.0) at a flow rate of 0.8 mL/min in line with a diode array detector (PerkinElmer, Wellesley, MA, USA) monitoring at 280 nm. Fab fragments were concentrated and buffer-exchanged into 50 mM NaHCO$_3$ buffer (pH 7.5) on an Amicon Ultracel 30 K device (M$_r$ cut-off = 30 kDa; Millipore Corp., Billerica, MA, USA). Trace metals were removed from all buffers using Chelex-100 cation-exchange resin (BioRad). The final Fab fragments concentration was measured spectrophotometrically [E$_{280\ nm}$ = 1.45 (mg/mL)$^{-1}$ cm$^{-1}$] [7] and was adjusted to 5 mg/mL with 50 mM NaHCO$_3$ buffer, pH 7.5.

## DOTA conjugation and radiolabeling of Fab fragments

Trastuzumab or rituximab Fab fragments were modified with DOTA for complexing ^{111}In or ^{64}Cu by reaction of 1.5 mg of Fab in 300 μL of NaHCO$_3$ buffer (pH 7.5) with a 60- or 90-fold excess, respectively, of the N-hydroxysuccinimidyl ester of 1,4,7,10-tetraazacyclododecane tetraacetic acid (NHS-DOTA; Macrocyclics, Dallas, TX, USA). The conjugation reaction was performed at

4°C for 18 h. DOTA-conjugated Fab were purified from excess DOTA by transferring to an Amicon Ultracel 30 K device, diluting to 12.0 mL with 1 M $CH_3COONH_4$ buffer, pH 6.0 and centrifuging at 4,000 × $g$ for 15 min. This purification step was repeated six times. Finally, purified DOTA-Fab were recovered and the concentration determined spectrophotometrically [$E_{280\ nm}$ = 1.45 (mg/mL)$^{-1}$ cm$^{-1}$]. The final concentration was adjusted to 5 mg/mL with 1 M $CH_3COONH_4$ buffer, pH 6.0.

Radiolabeling was performed by incubating 50 μg of DOTA-Fab in 10 μL of $CH_3COONH_4$ buffer, pH 6.0 with 360 MBq of $^{111}InCl_3$ (> 7 GBq/mL; MDS-Nordion, Kanata, ON, Canada) or 216 MBq of $^{64}CuCl_2$ (> 4 GBq/mL; MDS-Nordion) for 3 h at 46°C. $^{111}$In- or $^{64}$Cu-labeled DOTA-Fab were purified on an Amicon Ultracel 30 K device. The final radiochemical purity was measured by instant thin layer-silica gel chromatography (ITLC-SG; Pall Life Sciences, Ann Arbor, MI, USA) developed in 100 mM sodium citrate, pH 5.0 or by size-exclusion HPLC using a flow-through radioactivity detector (FSA; PerkinElmer). The $R_f$ values for $^{111}$In- or $^{64}$Cu-DOTA-Fab on ITLC were 0.0 and those for $^{111}$In- or $^{64}$Cu-DOTA or free radionuclides were 1.0. The DOTA substitution level of the Fab fragments (chelators/molecule) was measured by labeling a 10 μL aliquot of the unpurified conjugation reaction with $^{111}$In, then determining the proportion of $^{111}$In-DOTA-Fab *vs.* free $^{111}$In-DOTA by ITLC-SG and multiplying this fraction by the molar ratio used in the reaction [26].

### HER2 binding affinity of $^{111}$In- and $^{64}$Cu-DOTA-trastuzumab Fab

The HER2 binding affinity of $^{111}$In- and $^{64}$Cu-DOTA-trastuzumab Fab was determined by direct (saturation) radioligand binding assays using SKBR-3 human BC cells (1.3 × 10$^6$ HER2/cell) [9]. Briefly, increasing concentrations (0 to 600 nmol/L) of $^{111}$In- or $^{64}$Cu-DOTA-trastuzumab Fab were incubated with 1 × 10$^5$ cells in 24-well plates at 4°C for 3 h. Unbound radioactivity was removed and the dishes were rinsed two times with phosphate-buffered saline. The cells were dissolved in 100 mM NaOH, recovered, and the total cell-bound radioactivity (TB) was measured in a γ-counter (PerkinElmer Wizard 3). The assay was repeated in the presence of 16 μmol/L of unlabeled trastuzumab IgG to measure non-specific binding (NSB). Specific binding (SB; nanomoles per liter) was calculated by subtracting NSB from TB and was plotted *vs.* the concentration of $^{111}$In- or $^{64}$Cu-DOTA-trastuzumab Fab (nanomoles per liter) added. The resulting curve was fitted by non-linear regression to a one-site receptor-binding model by Prism Ver. 4.0 software (GraphPad, San Diego, CA, USA). The dissociation constant ($K_d$) and maximum number of receptors per cell ($B_{max}$) were calculated and compared for $^{111}$In- and $^{64}$Cu-DOTA-trastuzumab Fab.

### Tumor and normal tissue distribution studies

The tumor and normal tissue distribution of $^{111}$In- or $^{64}$Cu-DOTA-trastuzumab Fab were determined at 24-h post-intravenous (tail vein) injection (p.i.) in athymic mice with s.c. human tumor xenografts with a wide range of HER2 density. This time point was selected due to the short physical half-life of $^{64}$Cu (12.7 h) and because high tumor uptake [> 5 percent injected dose per gram (% i.d./g)] and tumor/blood ($T/B$) ratios (> 4:1) were previously found for $^{111}$In-DTPA-trastuzumab Fab at 24 h p.i. [7]. Tumors were established in female athymic (CD1-nude) mice by s.c. inoculation of 1 × 10$^7$ MDA-MB-231, BT-20, or MDA-MB-361 BC cells expressing 5.4 × 10$^4$, 1.6 × 10$^5$, or 5.1 × 10$^5$ HER2/cell, respectively, or with SK-OV-3 ovarian cancer cells displaying 1.2 × 10$^6$ HER2/cell [27]. At 4 to 7 weeks post-inoculation, when tumors were well established (5 to 15 mm in diameter), groups of mice ($n$ = 4) were injected i.v. (tail vein) with 12 MBq (10 μg) of $^{111}$In-DOTA-trastuzumab Fab or 18 MBq (10 μg) of $^{64}$Cu-DOTA-trastuzumab Fab. To determine if tumor uptake was specific, control groups of mice ($n$ = 4) with MDA-MB-231, BT-20, or MDA-MB-361 xenografts were injected i.v. with 12 MBq (10 μg) of irrelevant $^{111}$In-DOTA-rituximab Fab or 18 MBq (10 μg) of $^{64}$Cu-DOTA-rituximab Fab. Mice were euthanized by cervical dislocation under general anaesthesia. Tumor and normal tissue uptake of radioactivity was measured in a γ-scintillation counter (Wizard 3, PerkinElmer, Waltham, MA) was expressed as percent injected dose per gram and as tumor/normal tissue ($T/NT$) ratios. The relationship between tumor/blood ($T/B$) ratios and HER2 density was examined. The uptake of $^{111}$In- or $^{64}$Cu-DOTA-trastuzumab Fab fragments in small (5 to 10 mm diameter) *vs.* larger (10 to 15 mm diameter) tumor xenografts was compared.

### MicroSPECT and microPET imaging

MicroSPECT was performed at 24 h p.i. of 70 MBq (10 μg) of $^{111}$In-DOTA-trastuzumab Fab or $^{111}$In-DOTA-rituximab Fab in athymic mice with s.c. HER2-positive tumor xenografts. Anaesthesia was induced and maintained by inhalation of 2% isoflurane in $O_2$. MicroSPECT was performed on a NanoSPECT/CT tomograph (Bioscan, Washington, DC, USA) equipped with four NaI scintillation detectors fitted with 1.4-mm multi-pinhole collimators [full-width half-maximum (FWHM) = 1.2 mm]. A total of 24 projections were acquired in a 256 × 256 matrix with a minimum of 80,000 counts per projection. MicroSPECT image acquisition time was 85 to 120 mins. MicroSPECT images were reconstructed using an ordered-subset expectation maximization (OSEM) algorithm (nine

iterations). Prior to microSPECT imaging, cone-beam CT images were acquired (180 projections, 1 s/projection, 45 kVp) on the NanoSPECT/CT system. Co-registration of microSPECT and CT images was performed using Invivo-Scope software (Bioscan).

MicroPET was performed at 24 h p.i. of 22 MBq (10 μg) of $^{64}$Cu-DOTA-trastuzumab Fab or $^{64}$Cu-DOTA-rituximab Fab on a Focus 220 microPET tomograph (Siemens Preclinical Solutions, Knoxville, TN, USA). Images were acquired for 20 mins and reconstructed using OSEM, followed by a maximum *a posteriori* probability reconstruction algorithm with no correction for attenuation or partial-volume effects. The FWHM resolution of the microPET tomograph was 1.6 mm. Immediately after imaging, CT was performed on an eXplore Locus Ultra Preclinical CT scanner (GE Healthcare, Mississauga, ON, Canada) with routine acquisition parameters (80 kVp, 70 mA, and voxel size of 150 × 150 × 150 mm). MicroPET and CT images were coregistered using Inveon Research Workplace software (Siemens). All animal studies were conducted under a protocol (no. 989.9) approved by the Animal Use Committee at the University Health Network following Canadian Council on Animal Care guidelines.

### Statistical analyses

Statistical significance of comparisons were assessed by Student's *t* test ($P < 0.05$).

## Results
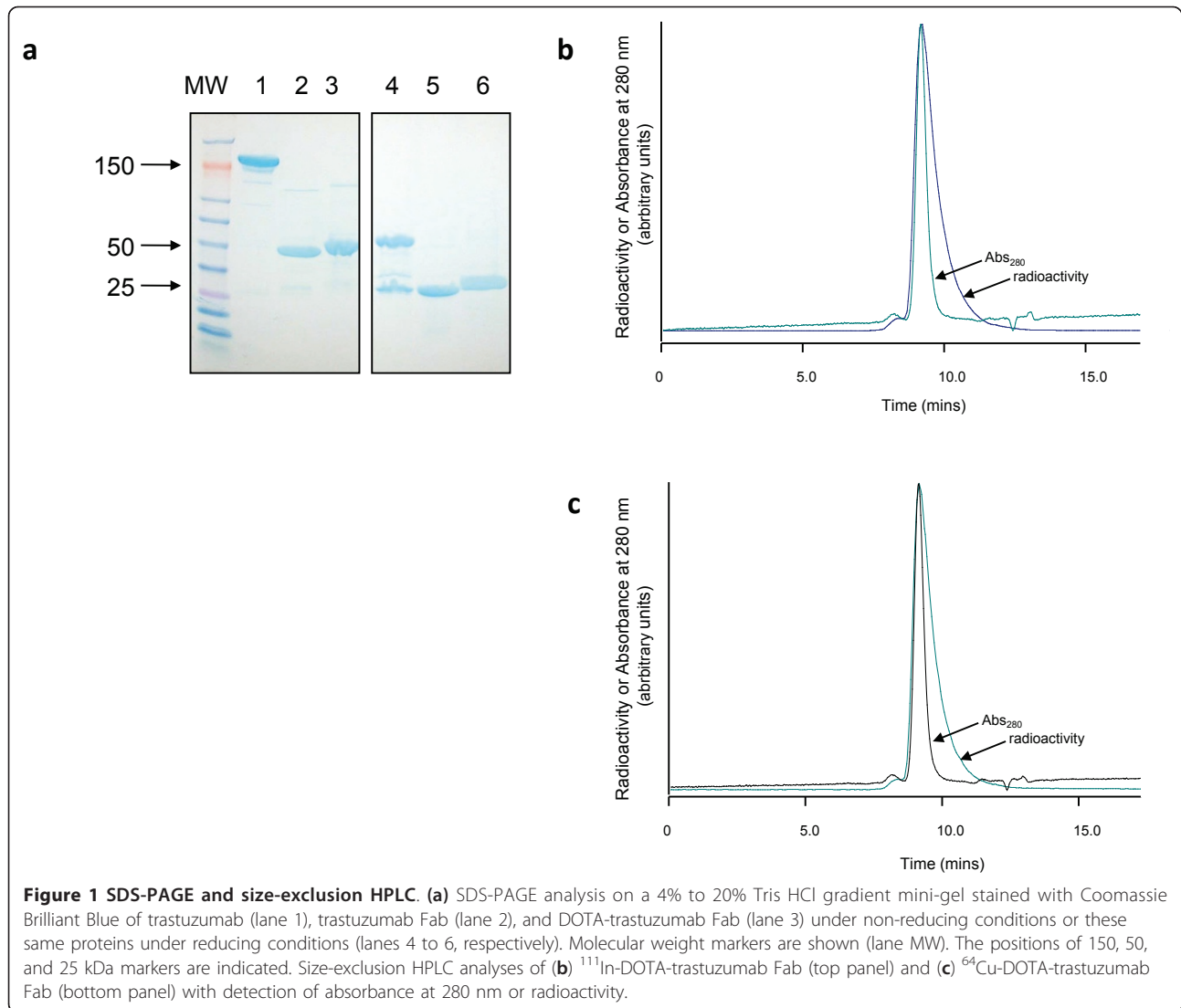### Preparation of $^{111}$In and $^{64}$Cu-labeled DOTA-Fab fragments

SDS-PAGE (Figure 1a) and size-exclusion HPLC (Figure 1b,c) demonstrated that pure (> 98%) Fab fragments of trastuzumab and rituximab were obtained by digestion of intact IgG$_1$ with immobilized papain using a previously reported method [7,25]. Reaction of trastuzumab and rituximab Fab with a 60- or 90-fold excess of NHS-DOTA for 18 h at 4°C resulted in substitution of 3.7 ± 0.2 and 2.5 ± 0.3 DOTA chelators per molecule, respectively. The pre-purification labeling efficiencies for $^{111}$In-DOTA-trastuzumab Fab, $^{111}$In-DOTA-rituximab Fab, $^{64}$Cu-DOTA-trastuzumab Fab, and $^{64}$Cu-DOTA-rituximab Fab were 75.5 ± 5.4%, 76.8 ± 1.5%, 65.9 ± 4.9%, and 67.9 ± 5.7%, respectively. Following purification, the radiochemical purity was > 98% for all radioimmunoconjugates by ITLC (not shown) and size-exclusion HPLC (Figure 1b,c). The specific activities of $^{111}$In- and $^{64}$Cu-DOTA-trastuzumab Fab fragments used in microSPECT and microPET and biodistribution studies were 3.6 to 4.9 MBq/μg and 1.3 to 4.7 MBq/μg, respectively. The specific activities of $^{111}$In- and $^{64}$Cu-DOTA-rituximab Fab were 1.3 to 5.8 and 1.9 to 2.8 MBq/μg.

### HER2 binding affinity of $^{111}$In- and $^{64}$Cu-DOTA-trastuzumab Fab

Direct (saturation) radioligand binding assays showed that $^{111}$In- and $^{64}$Cu-DOTA-trastuzumab Fab bound specifically to HER2 on SKBR-3 cells (Figure 2a,b). The $K_d$ values for $^{111}$In- and $^{64}$Cu-DOTA-trastuzumab Fab were 20.4 ± 2.5 nM and 40.8 ± 3.5 nM ($P < 0.01$), respectively. These values were similar to the $K_d$ for $^{111}$In-DTPA-trastuzumab Fab binding to SKBR-3 cells previously reported by our group ($K_d$ = 48 nM) [25]. There was no specific binding of $^{111}$In-DOTA-rituximab to SKBR-3 cells (not shown). The $B_{max}$ values for $^{111}$In- and $^{64}$Cu-DOTA-trastuzumab Fab on SKBR-3 cells were 1.4 ± 0.1 × 10$^6$ receptors/cell and 2.3 ± 0.1 × 10$^6$ receptors/cell, respectively ($P < 0.001$).

### Tumor and normal tissue distribution studies

The tumor and normal tissue uptake of $^{111}$In- and $^{64}$Cu-DOTA-trastuzumab Fab at 24 h p.i. in athymic mice bearing s.c. MDA-MB-361 human BC xenografts (5.1 × 10$^5$ HER2/cell) are shown in Table 1. Blood levels were threefold significantly higher for $^{64}$Cu- than $^{111}$In-DOTA-trastuzumab Fab (1.40 ± 0.16% *vs.* 0.42 ± 0.08% i.d./g; $P < 0.0001$). Similarly, liver uptake was threefold significantly greater for $^{64}$Cu- than $^{111}$In-DOTA-trastuzumab Fab (8.52 ± 0.81% *vs.* 3.13 ± 0.15% i.d./g; $P < 0.0001$). Radioactivity concentrations were higher in heart, lungs, stomach, intestines, and spleen for $^{64}$Cu- than $^{111}$In-DOTA-trastuzumab Fab (Table 1). However, kidney uptake was not significantly different between $^{64}$Cu- and $^{111}$In-DOTA-trastuzumab Fab (57.00 ± 7.09% *vs.* 62.85 ± 6.45% i.d./g; $P = 0.268$). There was no significant difference in tumor accumulation for $^{111}$In- and $^{64}$Cu-DOTA-trastuzumab Fab (4.00 ± 0.90% *vs.* 5.00 ± 1.2% i.d./g; $P = 0.228$). Due to the higher blood and liver radioactivity, the $T/B$ and tumor/liver ($T/L$) ratios were three- and twofold significantly lower, respectively for $^{64}$Cu- than $^{111}$In-DOTA-trastuzumab Fab (3.56 ± 0.62 *vs.* 9.73 ± 2.46; $P = 0.003$ and 0.59 ± 0.16 *vs.* 1.27 ± 0.26 *vs.*; $P = 0.004$, respectively; Table 2). $T/NT$ ratios for $^{64}$Cu-DOTA-trastuzumab Fab were significantly lower than $^{111}$In-DOTA-trastuzumab Fab for all tissues except kidneys and muscle (Table 2). There was no significant difference in the uptake of $^{111}$In- or $^{64}$Cu-DOTA-trastuzumab Fab in small (5 to 10 mm diameter) *vs.* larger (10 to 15 mm) MDA-MB-361 tumor xenografts (4.00 ± 0.91% *vs.* 6.12 ± 0.84% i.d./g; $P = 0.138$ and 5.01 ± 1.20% *vs.* 7.12 ± 1.67% i.d./g, $P = 0.342$, respectively). Absolute tumor uptake was not informative on the relationship between tumor localization of the radioimmunoconjugates and HER2 expression. Tumor uptake of $^{111}$In-DOTA-trastuzumab in MDA-MB-231, BT-20, MDA-MB-361, or SKOV-3 xenografts
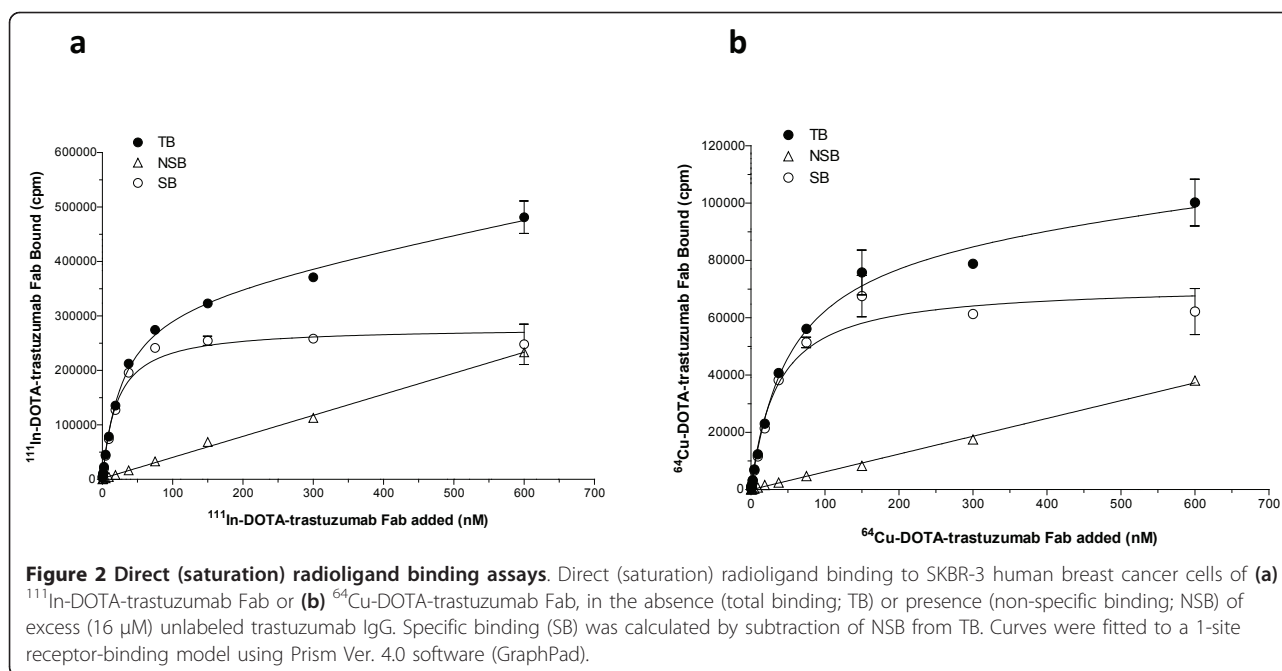
**Figure 1 SDS-PAGE and size-exclusion HPLC**. **(a)** SDS-PAGE analysis on a 4% to 20% Tris HCl gradient mini-gel stained with Coomassie Brilliant Blue of trastuzumab (lane 1), trastuzumab Fab (lane 2), and DOTA-trastuzumab Fab (lane 3) under non-reducing conditions or these same proteins under reducing conditions (lanes 4 to 6, respectively). Molecular weight markers are shown (lane MW). The positions of 150, 50, and 25 kDa markers are indicated. Size-exclusion HPLC analyses of (**b**) ^{111}In-DOTA-trastuzumab Fab (top panel) and (**c**) ^{64}Cu-DOTA-trastuzumab Fab (bottom panel) with detection of absorbance at 280 nm or radioactivity.

with increasing HER2 density was 4.7 ± 0.6%, 5.5 ± 0.7%, 4.0 ± 0.9%, and 5.4 ± 0.4% i.d./g. Tumor uptake of ^{64}Cu-DOTA-trastuzumab in MDA-MB-231, BT-20, MDA-MB-361, or SKOV-3 xenografts was 4.4 ± 1.6%, 2.6 ± 1.8%, 5.0 ± 1.2%, and 5.0 ± 3.0% i.d./g. However, there was a strong direct relationship between $T/B$ ratios for ^{111}In-DOTA-trastuzumab Fab and tumor HER2 density (Figure 3a). Moreover, the $T/B$ ratios for ^{111}In-DOTA-trastuzumab Fab were significantly greater than irrelevant ^{111}In-DOTA-rituximab Fab for MDA-MB-231, BT-20, and MDA-MB-361 xenografts, demonstrating specific localization. The $T/B$ ratios for ^{64}Cu-DOTA-trastuzumab Fab were significantly greater than ^{64}Cu-DOTA-rituximab Fab for MDA-MB-361 tumors with high HER2 density ($P < 0.001$), but not for MDA-MB-231 or BT-20 xenografts with low HER2 expression ($P = 0.0709$ and 0.528, respectively; Figure 3b). The

localization of [111]In- or ^{64}Cu-DOTA-rituximab Fab in SK-OV-3 tumors was not determined. No relationship between the $T/B$ ratios for ^{64}Cu-DOTA-trastuzumab Fab and HER2 density was established (Figure 3b).

### MicroSPECT/CT and microPET/CT imaging
Representative microSPECT and microPET images of athymic mice with s.c. tumor xenografts with increasing HER2 density at 24 h p.i. of [111]In- or ^{64}Cu-DOTA-trastuzumab Fab, respectively are shown in Figures 4 and 5. MicroSPECT/CT and microPET/CT images were displayed as coronal slices with the plane selected to optimally display the tumor uptake of ^{111}In-DOTA-trastuzumab Fab or ^{64}Cu-DOTA-trastuzumab Fab. MDA-MB-231 tumors with low HER2 expression ($5.4 \times 10^4$ receptors/cell; Figures 4a and 5a) were least intensely imaged while SK-OV-3 tumors with high HER2 density

**Figure 2 Direct (saturation) radioligand binding assays**. Direct (saturation) radioligand binding to SKBR-3 human breast cancer cells of **(a)** ^{111}In-DOTA-trastuzumab Fab or **(b)** ^{64}Cu-DOTA-trastuzumab Fab, in the absence (total binding; TB) or presence (non-specific binding; NSB) of excess (16 μM) unlabeled trastuzumab IgG. Specific binding (SB) was calculated by subtraction of NSB from TB. Curves were fitted to a 1-site receptor-binding model using Prism Ver. 4.0 software (GraphPad).

(1.2 × 10^{6} receptors/cell) were most clearly seen (Figures 4c and 5c) with [111]In- or ^{64}Cu-DOTA-trastuzumab. An intermediate tumor signal was found for MDA-MB-361 xenografts with 5.1 × 10^{5} HER2/cell (Figures 4b and 5b). The specificity of tumor localization of [111]In- or ^{64}Cu-DOTA-trastuzumab Fab was shown by the lower accumulation of [111]In- or ^{64}Cu-DOTA-rituximab Fab on images of mice bearing MDA-MB-361 xenografts (Figures 4d and 5d). There was no difference in the ability of [111]In- or ^{64}Cu-DOTA-trastuzumab Fab to image small (5 to 10 mm; Figure 6a,c) or larger (10 to 15 mm;

Figure 6b, d) MDA-MB-361 tumors. The kidneys were most prominent on microSPECT images of ^{111}In-DOTA-trastuzumab Fab, while microPET with ^{64}Cu-DOTA-trastuzumab Fab showed high liver and kidney uptake.

## Discussion

Our results revealed that both microSPECT/CT and microPET/CT with [111]In- or ^{64}Cu-DOTA-trastuzumab Fab fragments were able to image s.c. human tumor xenografts in mice with low, intermediate, or high HER2

**Table 1 Tumor and normal tissue distribution at 24 h post-injection of [111]In- or ^{64}Cu-DOTA-trastuzumab Fab**

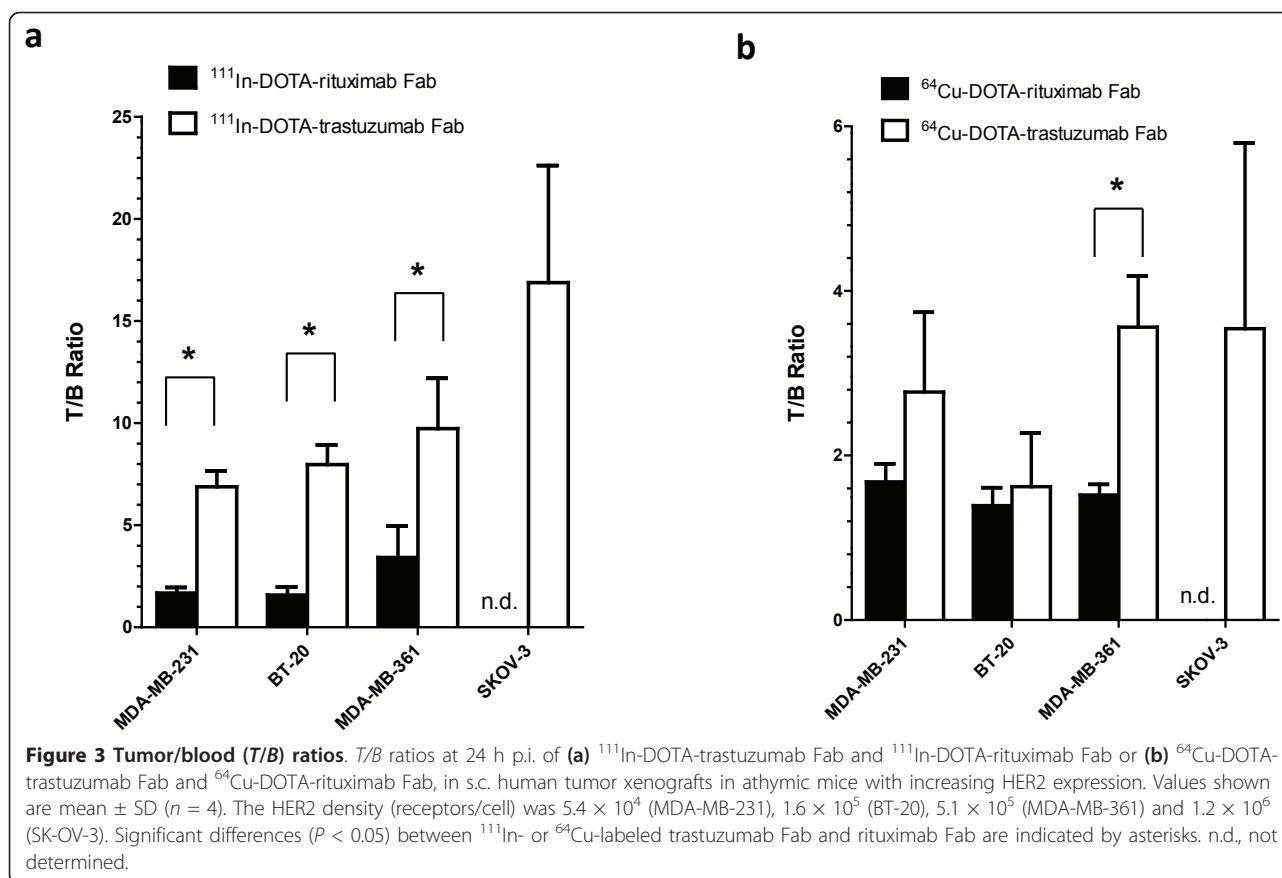| Tissue | Percent injected dose/g [a, b, c] | |
| --- | --- | --- |
| | ^{111}In-DOTA-trastuzumab Fab | ^{64}Cu-DOTA-trastuzumab Fab |
| Blood | 0.42 ± 0.08 | 1.40 ± 0.16 |
| Heart | 0.92 ± 0.06 | 2.42 ± 0.39 |
| Lungs | 0.80 ± 0.14 | 4.86 ± 0.57 |
| Liver | 3.13 ± 0.16 | 8.52 ± 0.81 |
| Kidneys | 62.85 ± 6.45 | 57.00 ± 7.09 |
| Stomach | 0.58 ± 0.05 | 3.41 ± 0.22 |
| Intestines | 0.61 ± 0.06 | 4.76 ± 0.41 |
| Spleen | 2.25 ± 0.13 | 5.00 ± 0.27 |
| Muscle | 0.78 ± 0.31 | 0.75 ± 0.06 |
| Tumor | 4.00 ± 0.91 | 5.01 ± 1.20 |

[111]In- or ^{64}Cu-DOTA-trastuzumab Fab in athymic mice bearing subcutaneous MDA-MB-361 human breast cancer xenografts. [a]Values shown are mean ± SD (n = 4). [b]Significantly different for [111]In- and ^{64}Cu-DOTA-trastuzumab Fab for blood, heart, lungs, liver, stomach, intestines, and spleen (all *P* < 0.001). [c]Not significantly different for [111]In- and ^{64}Cu-DOTA-trastuzumab Fab for kidneys, muscle, or tumor (*P* > 0.05).

**Table 2 Tumor/normal tissue (T/NT) ratios at 24 h post-injection of [111]In- or ^{64}Cu-DOTA-trastuzumab Fab**

| Tissue | T/NT Ratio [a, b, c] | |
| --- | --- | --- |
| | ^{111}In-DOTA-trastuzumab Fab | ^{64}Cu-DOTA-trastuzumab Fab |
| Blood | 9.73 ± 2.46 | 3.56 ± 0.62 |
| Heart | 4.31 ± 0.83 | 2.09 ± 0.56 |
| Lungs | 5.06 ± 1.12 | 1.03 ± 0.19 |
| Liver | 1.27 ± 0.26 | 0.59 ± 0.16 |
| Kidneys | 0.06 ± 0.02 | 0.09 ± 0.02 |
| Stomach | 6.99 ± 2.05 | 1.48 ± 0.37 |
| Intestines | 6.61 ± 1.78 | 1.05 ± 0.22 |
| Spleen | 1.79 ± 0.48 | 1.00 ± 0.20 |
| Muscle | 6.12 ± 3.33 | 6.78 ± 1.90 |

[111]In- or ^{64}Cu-DOTA-trastuzumab Fab in athymic mice bearing subcutaneous MDA-MB-361 human breast cancer xenografts. [a]Values shown are mean ± SD (n = 4). [b]Significantly different for [111]In- and ^{64}Cu-DOTA-trastuzumab Fab for lungs and intestines (both *P* < 0.001), blood, heart, liver, stomach (all *P* < 0.01) and spleen (*P* < 0.05). [c]Not significantly different for [111]In- and ^{64}Cu-DOTA-trastuzumab Fab for kidneys and muscle (*P* > 0.05).

**Figure 3 Tumor/blood (*T/B*) ratios**. *T/B* ratios at 24 h p.i. of **(a)** ^{111}In-DOTA-trastuzumab Fab and ^{111}In-DOTA-rituximab Fab or **(b)** ^{64}Cu-DOTA-trastuzumab Fab and ^{64}Cu-DOTA-rituximab Fab, in s.c. human tumor xenografts in athymic mice with increasing HER2 expression. Values shown are mean ± SD (*n* = 4). The HER2 density (receptors/cell) was $5.4 \times 10^4$ (MDA-MB-231), $1.6 \times 10^5$ (BT-20), $5.1 \times 10^5$ (MDA-MB-361) and $1.2 \times 10^6$ (SK-OV-3). Significant differences (*P* < 0.05) between [111]In- or ^{64}Cu-labeled trastuzumab Fab and rituximab Fab are indicated by asterisks. n.d., not determined.

expression. The range of HER2 expression examined ($5.4 \times 10^4$ to $1.2 \times 10^6$ receptors/cell) corresponded to HER2 scores of 0 to 3+ assessed clinically in BC specimens by IHC staining [9]. There was no apparent increased ability of microPET/CT with ^{64}Cu-DOTA-trastuzumab Fab compared to microSPECT/CT with ^{111}In-DOTA-trastuzumab Fab to visualize MDA-MB-231 tumors with low HER2 density ($1.6 \times 10^5$ receptors/cell; Figures 4a and 5a). In addition, there was no increased ability of microPET/CT using ^{64}Cu-DOTA-trastuzumab Fab to image small (5 to 10 mm diameter) or larger (10 to 15 mm diameter) MDA-MB-361 tumors with intermediate HER2 expression ($5.1 \times 10^5$ HER2/cell; Figure 6). The intensity of the tumor signal was dependent on HER2 expression with tumors with intermediate (MDA-MB-361) or high (SK-OV-3) HER2 density most readily imaged by microSPECT/CT (Figure 4) or microPET/CT (Figure 5). However, a threefold higher dose of radioactivity was administered for microSPECT/CT than microPET/CT (70 *vs.* 22 MBq) and image acquisition times were up to sixfold longer for microSPECT/CT (85 to 20 *vs.* 20 min, respectively). Thus, the photon detection efficiency (i.e., intrinsic sensitivity) was much higher for microPET/CT than microSPECT/CT. Nonetheless, our results revealed that provided that the administered dose of radioactivity was sufficient and image acquisition times were long enough to yield good counting statistics, microSPECT/CT with ^{111}In-DOTA-trastuzumab Fab was able to image tumors with the similar HER2 density and size as microPET/CT with ^{64}Cu-DOTA-trastuzumab. These results agree with those reported by Cheng et al. who noted that s.c. HER2-positive SUM190 tumor xenografts were imaged by either microSPECT or microPET using trastuzumab conjugated to biotinylated [99 m]Tc- or ^{18}F-labeled phospho-diamidate morpholinos (MORFs) through a streptavidin linker [28]. The doses of [99 m]Tc or ^{18}F used in their study were 13 and 0.22 MBq, respectively. Phantom studies revealed that microPET was 15-fold more sensitive in terms of photon detection, but the spatial resolution of microSPECT was superior to that of microPET (1.2 *vs.* 2.4 mm). The results are also in concordance with those reported by Wong et al. [29], who showed that s.c. epidermal growth factor receptor-positive LS174T human colon cancer xenografts could be imaged using panitumomab F(ab')$_2$ fragments labeled with ^{111}In or [86]Y. However, they compared low resolution planar γ-camera imaging with microPET. In our study, we used similar quality high resolution and high sensitivity small animal imaging technologies, namely microSPECT/CT (NanoSPECT; Bioscan) and
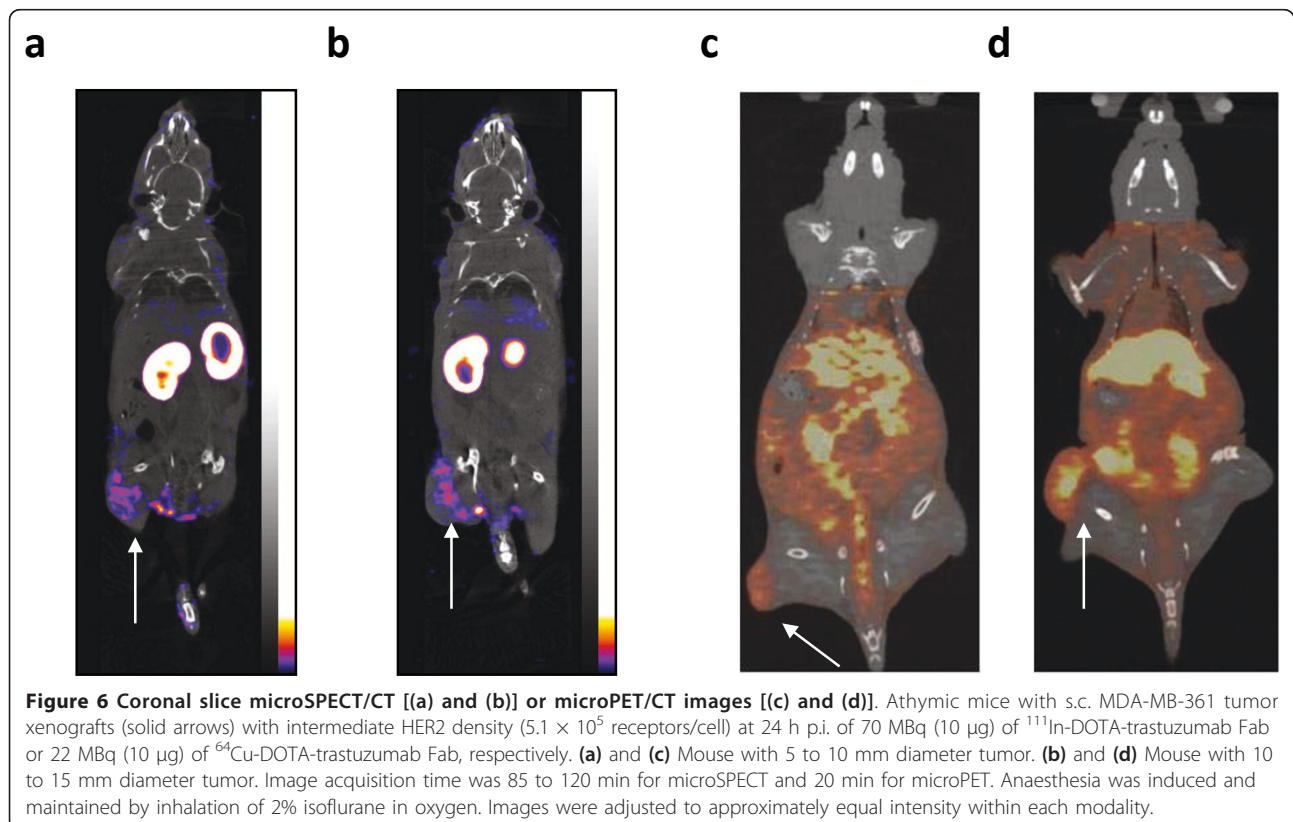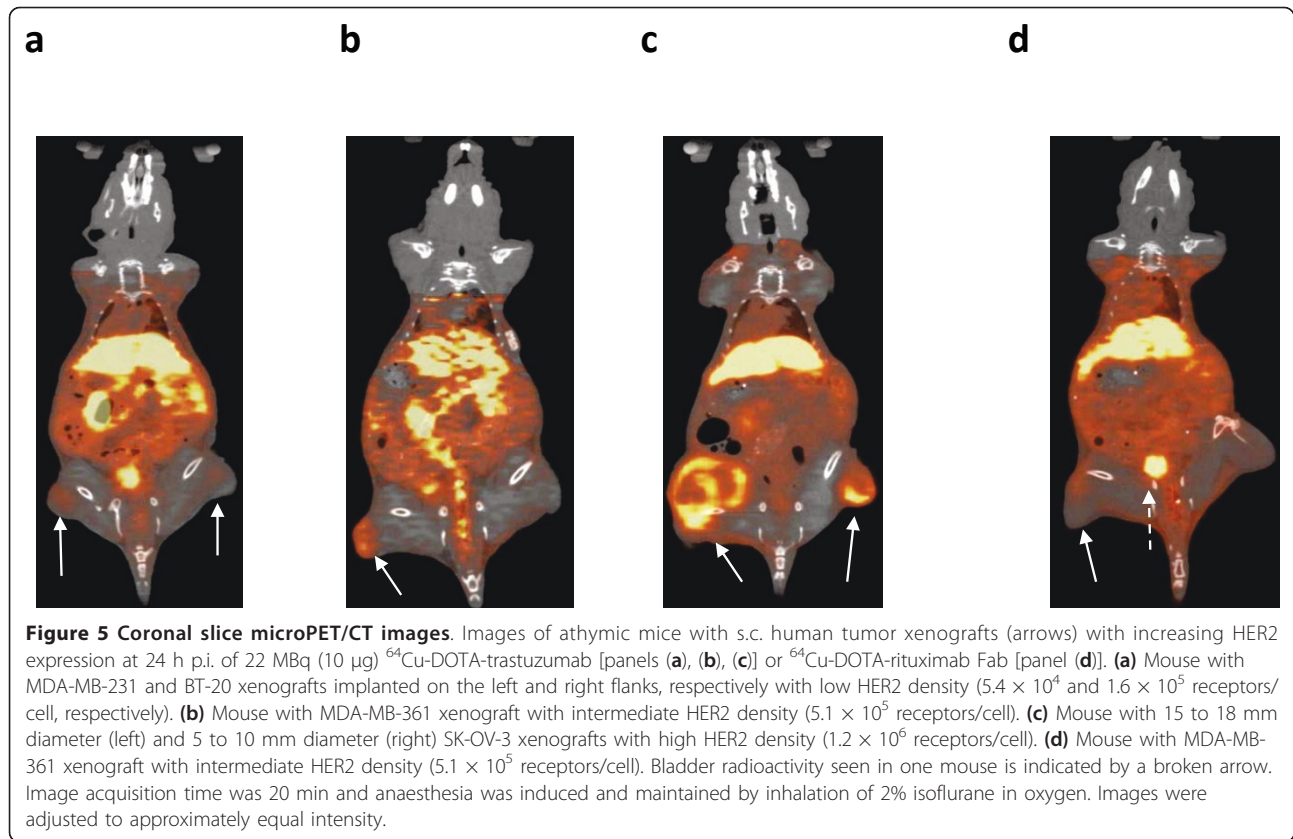
**Figure 4 Coronal slice microSPECT/CT images**. Images of athymic mice with s.c. human tumor xenografts (solid arrows) with increasing HER2 expression at 24 h p.i. of 70 MBq (10 μg) of ^{111}In-DOTA-trastuzumab [panels (**a**), (**b**), (**c**)] or ^{111}In-DOTA-rituximab Fab [panel (**d**)]. (**a**) Mouse with MDA-MB-231 (left panel) and BT-20 (right panel) xenografts with low HER2 density ($5.4 \times 10^4$ and $1.6 \times 10^5$ receptors/cell, respectively). (**b**) Mouse with MDA-MB-361 xenograft with intermediate HER2 density ($5.1 \times 10^5$ receptors/cell). (**c**) Mouse with 15 to 18 mm diameter (left flank) and 5 to 10 mm diameter (right flank) SK-OV-3 xenografts with high HER2 density ($1.2 \times 10^6$ receptors/cell). (**d**) Mouse with MDA-MB-361 xenograft with intermediate HER2 density ($5.1 \times 10^5$ receptors/cell). Bladder radioactivity in panel (c) is indicated by broken arrow. Image acquisition time was 85 to 120 min and anaesthesia was induced and maintained by inhalation of 2% isoflurane in oxygen. Images were adjusted to approximately equal intensity.

microPET (Siemens Focus 220) systems for these comparisons.

$T/B$ ratios were used to compare the tumor localization of [111]In- and ^{64}Cu-DOTA-trastuzumab Fab *vs.* HER2 density because we previously found that there are differences in perfusion between different tumor xenografts which can affect the uptake of radioimmunoconjugates [9]. Use of $T/B$ ratios minimizes these effects by normalizing for blood concentrations which then reveals the relationships between HER2 density and tumor accumulation. Moreover, the $T/B$ ratios are important for discriminating tumors that have different HER2 expression on the images. There was a strong and direct association between the $T/B$ ratios for ^{111}In-DOTA-trastuzumab and tumor HER2 density (Figure 3a). In addition, the $T/B$ ratios for ^{111}In-DOTA-trastuzumab Fab were significantly greater than those of irrelevent control ^{111}In-DOTA-rituximab Fab for MDA-MB-231, BT-20, and MDA-MB-361 xenografts, demonstrating specific localization in tumors with low or intermediate HER2 expression. In contrast, specific uptake of ^{64}Cu-DOTA-trastuzumab Fab was shown in MDA-MB-361 tumors with intermediate HER2 density but not for tumors with lower HER2 expression (Figure 3b). Tumor uptake was not significantly different for [64]Cu- and ^{111}In-DOTA-trastuzumab Fab, but blood

radioactivity was threefold lower for ^{111}In-DOTA-trastuzumab Fab (Table 1). Thus, $T/B$ ratios were threefold lower for [64]Cu- than ^{111}In-DOTA-trastuzumab (3.6:1 *vs.* 10:1; Table 2) in mice with MDA-MB-361 tumors. The increased circulating radioactivity for ^{64}Cu-DOTA-trastuzumab Fab may be due to kinetic instability of the ^{64}Cu-DOTA complex with transchelation of released ^{64}Cu to copper binding proteins (e.g., albumin, ceruloplasmin, or superoxide dismutase) [26]. These ^{64}Cu-labeled proteins may non-specifically localize in tumors, disrupting the association between $T/B$ ratios and HER2 density, especially for tumors with low HER2 expression (i.e., MDA-MB-231 and BT-20).

DOTA forms thermodynamically stable complexes with copper ($K_d = 10^{23}$ M$^{-1}$) but kinetic instability of ^{64}Cu-DOTA complexes *in vivo* can lead to loss of radiometal resulting in high blood radioactivity and liver and spleen uptake [17]. In addition to the higher levels of blood radioactivity, we found that the liver and spleen uptake for ^{64}Cu-DOTA-trastuzumab Fab were three- and twofold greater, respectively, than ^{111}In-DOTA-trastuzumab Fab (Table 1). In order to improve the kinetic stability of ^{64}Cu complexes, more thermodynamically stable cross-bridged (CB-DO2A) or sarcophagine (SarAr) chelators have been synthesized [30,31]. A comparison of ^{64}Cu complexed to

**Figure 5 Coronal slice microPET/CT images**. Images of athymic mice with s.c. human tumor xenografts (arrows) with increasing HER2 expression at 24 h p.i. of 22 MBq (10 μg) $^{64}$Cu-DOTA-trastuzumab [panels (**a**), (**b**), (**c**)] or $^{64}$Cu-DOTA-rituximab Fab [panel (**d**)]. (**a**) Mouse with MDA-MB-231 and BT-20 xenografts implanted on the left and right flanks, respectively with low HER2 density ($5.4 \times 10^4$ and $1.6 \times 10^5$ receptors/cell, respectively). (**b**) Mouse with MDA-MB-361 xenograft with intermediate HER2 density ($5.1 \times 10^5$ receptors/cell). (**c**) Mouse with 15 to 18 mm diameter (left) and 5 to 10 mm diameter (right) SK-OV-3 xenografts with high HER2 density ($1.2 \times 10^6$ receptors/cell). (**d**) Mouse with MDA-MB-361 xenograft with intermediate HER2 density ($5.1 \times 10^5$ receptors/cell). Bladder radioactivity seen in one mouse is indicated by a broken arrow. Image acquisition time was 20 min and anaesthesia was induced and maintained by inhalation of 2% isoflurane in oxygen. Images were adjusted to approximately equal intensity.



**Figure 6 Coronal slice microSPECT/CT [(a) and (b)] or microPET/CT images [(c) and (d)]**. Athymic mice with s.c. MDA-MB-361 tumor xenografts (solid arrows) with intermediate HER2 density ($5.1 \times 10^5$ receptors/cell) at 24 h p.i. of 70 MBq (10 μg) of $^{111}$In-DOTA-trastuzumab Fab or 22 MBq (10 μg) of $^{64}$Cu-DOTA-trastuzumab Fab, respectively. (**a**) and (**c**) Mouse with 5 to 10 mm diameter tumor. (**b**) and (**d**) Mouse with 10 to 15 mm diameter tumor. Image acquisition time was 85 to 120 min for microSPECT and 20 min for microPET. Anaesthesia was induced and maintained by inhalation of 2% isoflurane in oxygen. Images were adjusted to approximately equal intensity within each modality.

DOTA or CB-DO2A (but not conjugated to mAbs) showed fourfold lower radioactivity in the blood and twofold lower liver accumulation at 24 h p.i. in rats [30]. Voss et al. noted that ch14.18 mAbs labeled with $^{64}$Cu through the extremely stable SarAr chelator for PET imaging of neuroblastoma or melanoma xenografts in mice exhibited low liver uptake (5% to 10% i.d./g) but no comparison with other chelators was provided [31]. Dearling et al. recently compared the tumor and normal tissue distribution of these same $^{64}$Cu-labeled ch14.18 mAbs using a variety of chelators including DOTA and SarAr in mice bearing M21 melanoma xenografts [17]. Unexpectedly, no significant differences in tumor or liver uptake were found for ch14.18 labeled with $^{64}$Cu using DOTA or the much more stable SarAr chelator. They suggested that in addition to $^{64}$Cu-chelator stability, factors such as the net charge on the chelators may play an important role in sequestration of radioactivity by tissues. In our study, tumor uptake was not significantly different between $^{111}$In- and $^{64}$Cu-DOTA-trastuzumab Fab in mice with MDA-MB-361 tumors, despite the apparent instability of $^{64}$Cu-DOTA-trastuzumab Fab as evidenced by higher levels of radioactivity in the blood, liver, and spleen (Table 1). The use of more stable chelators such as CB-DO2A or SarAr may diminish blood radioactivity and improve the association between tumor HER2 density and $T/B$ ratios for $^{64}$Cu-labeled trastuzumab Fab. The CB-DO2A and SarAr chelators are unfortunately not yet commercially available in a chemically reactive form for conjugation to mAbs for $^{64}$Cu labeling.

## Conclusion

Provided that administered doses of radioactivity and acquisition times were sufficient to yield good counting statistics, we conclude that either microSPECT/CT with $^{111}$In-DOTA-trastuzumab Fab or microPET/CT with $^{64}$Cu-DOTA-trastuzumab Fab visualized small (5 to 10 mm diameter) or larger (10 to 15 mm diameter) s.c. tumor xenografts with low, intermediate, or high HER2 expression in athymic mice. However, due to the higher levels of circulating radioactivity for $^{64}$Cu-DOTA-trastuzumab Fab, no association between HER2 density and $T/B$ ratios was established. In contrast, there was a strong direct association between $T/B$ ratios and HER2 density of these tumors for $^{111}$In-DOTA-trastuzumab Fab. Thus, $^{111}$In-DOTA-trastuzumab Fab was more specific than $^{64}$Cu-DOTA-trastuzumab Fab for imaging HER2-positive tumors with low HER2 density. The use of more stable CB-DO2A or SarAr chelators for $^{64}$Cu may potentially diminish blood radioactivity, provide a stronger association between $T/B$ ratios and tumor HER2 density, and improve the specificity of imaging with $^{64}$Cu-labeled trastuzumab Fab.

## Author details

$^1$Department of Pharmaceutical Sciences, University of Toronto, Toronto, M5S 3M2, ON, Canada $^2$Department of Medical Imaging, University of Toronto, Toronto, M5S 3E2, ON, Canada $^3$Toronto General Research Institute, University Health Network, Toronto, M5G 2M9, ON, Canada

## Authors' contributions

CC and SS synthesized the $^{111}$In- and $^{64}$Cu-DOTA-trastuzumab Fab fragments and performed characterization studies. KM and DAS performed microSPECT and microPET imaging studies. RMR wrote the manuscript with the assistance of all authors.

## Competing interests

The authors declare that they have no competing interests.

## References

1. Revillion F, Bonneterre J, Peyrat JP: **ERBB2 oncogene in human breast cancer and its clinical significance.** *Eur J Cancer* 1998, **34**:791-808.
2. Behr TM, Béhé M, Wörmann B: **Trastuzumab and breast cancer.** *N Engl J Med* 2001, **345**:995-996.
3. Owens MA, Horten BC, Da Silva MM: **HER2 amplification ratios by fluorescence** *in situ* **hybridization and correlation with immunohistochemistry in a cohort of 6556 breast cancer tissues.** *Clin Breast Cancer* 2004, **5**:63-69.
4. Munzone E, Nolé F, Goldhirsch A, Botteri E, Esposito A, Zorzino L, Curigliano G, Minchella I, Adamoli L, Cassatella MC, Casadio C, Sandri MT: **Changes in HER2 status in circulating tumor cells compared with the primary tumor during treatment for advanced breast cancer.** *Clin Breast Cancer* 2010, **10**:392-397.
5. Pestrin M, Bessi S, Gallardi F, Truglia M, Biggeri A, Biagioni C, Cappadona S, Biganzoli L, Giannini A, Di Leo A: **Correlation of HER2 status between primary tumors and corresponding circulating tumor cells in advanced breast cancer patients.** *Breast Cancer Res and Treatment* 2009, **118**:523-530.
6. Lub-de Hooge MN, Kosterink JG, Perik PJ, Nijnuis H, Tran L, Bart J, Suurmeijer AJH, de Jong S, Jager PL, de Vries EGE: **Preclinical characterisation of $^{111}$In-DTPA-trastuzumab.** *Br J Pharmacol* 2004, **143**:99-106.
7. Tang Y, Wang J, Scollard DA, Mondal H, Holloway C, Kahn HJ, Reilly RM: **Imaging of HER2/neu-positive BT-474 human breast cancer xenografts in athymic mice using $^{111}$In-trastuzumab (Herceptin) Fab fragments.** *Nucl Med Biol* 2005, **32**:51-58.
8. Tang Y, Scollard D, Chen P, Wang J, Holloway C, Reilly RM: **Imaging of HER2/neu expression in BT-474 human breast cancer xenografts in athymic mice using $^{99}$$^m$Tc-HYNIC-trastuzumab (Herceptin) Fab fragments.** *Nucl Med Commun* 2005, **26**:427-432.
9. McLarty K, Cornelissen B, Scollard DA, Done SJ, Chun K, Reilly RM: **Associations between the uptake of $^{111}$In-DTPA-trastuzumab, HER2 density and response to trastuzumab (Herceptin) in athymic mice bearing subcutaneous human tumour xenografts.** *Eur J Nucl Med Mol Imaging* 2009, **36**:81-93.
10. Perik PJ, Lub-de Hooge MN, Gietema JA, van der Graaf WTA, de Korte MA, Jonkman S, Kosterink JG, van Veldhuisen DJ, Sleijfer DT, Jager PL, de Vries EGE: **Indium-111-labeled trastuzumab scintigraphy in patients with human epidermal growth factor receptor 2-positive metastatic breast cancer.** *J Clin Oncol* 2006, **24**:2276-2282.
11. Dijkers EC, Oude Munnink TH, Kosterink JG, Brouwers AH, Jager PL de Jong R, van Dongen GA, Lub-de Hooge MN, de Vries EGE: **Biodistribution of $^{89}$Zr-trastuzumab and PET imaging of HER2-positive lesions in patients with metastatic breast cancer.** *Clin Pharmacol Ther* 2010, **87**:586-592.
12. Dijkers ECF, Kosterink JGW, Rademaker AP, Perk LR, van Dongen GA, Bart J, de Jong R, de Vries EGE, Lub-de Hooge MN: **Development and**

characterization of clinical-grade [89]Zr-trastuzumab for HER2/*neu* immunoPET imaging. *J Nucl Med* 2009, **50**:974-981.

13. McLarty K, Reilly RM: **Molecular imaging as a tool for personalized and targeted anticancer therapy.** *Clin Pharmacol Ther* 2007, **81**:420-424.

14. McLarty K, Cornelissen B, Scollard D, Reilly RM: **Micro-SPECT/CT with** [111]**In-DTPA-pertuzumab sensitively detects trastuzumab-mediated** *HER2* **downregulation and tumor response in athymic mice bearing MDA-MB-361 human breast cancer xenografts.** *J Nucl Med* 2009, **50**:1340-1348.

15. Smith-Jones PM, Solit DB, Akhurst T, Afroze F, Rosen N, Larson SM: **Imaging the pharmacodynamics of HER-2 degradation in response to Hsp90 inhibitors.** *Nat Biotechnol* 2004, **22**:701-706.

16. Garcia R, Kubicek V, Drahos B, Gano L, Santos IC, Campello P, Paulo A, Toth E, Santos I: **Synthesis, characterization and biological evaluation of In(III) complexes anchored by DOTA-like chelators bearing a quinazoline moiety.** *Metallomics* 2010, **2**:571-580.

17. Dearling JLJ, Voss SD, Dunning P, Snay E, Fahey F, Smith SV, Huston JS, Meares CF, Treves ST, Packard AB: **Imaging cancer using PET - the effect of the bifunctional chelator on the biodistribution of a** [64]**Cu-labeled antibody.** *Nucl Med Biol* 2011, **38**:29-38.

18. Olafsen T, Kenanova VE, Sundaresan G, Anderson AL, Crow D, Smith SV, Huston JS, Meares CF, Treves ST, Packard AB: **Optimizing radiolabeled engineered anti-p185HER2 antibody fragments for** *in vivo* **imaging.** *Cancer Res* 2005, **65**:5907-5916.

19. Cai W, Chen K, He L, Cao Q, Koong A, Chen X: **Quantitative PET of EGFR expression in xenograft-bearing mice using** [64]**Cu-labeled cetuximab, a chimeric anti-EGFR monoclonal antibody.** *Eur J Nucl Med Mol Imaging* 2007, **34**:850-858.

20. Niu G, LI Z, Cao Q, Chen X: **Monitoring therapeutic response of human ovarian cancer to 17-DMAG by non-invasive PET imaging with** [64]**Cu-DOTA-trastuzumab.** *Eur J Nucl Med Mol Imaging* 2009, **36**:1510-1519.

21. Anderson CJ, Dehdashti F, Cutler PD, Schwartz SW, LaForest R, Bass LA, Lewis JS, McCarthy DW: [64]**Cu-TETA-octreotide as a PET imaging agent for patients with neuroendocrine tumors.** *J Nucl Med* 2001, **42**:213-221.

22. Rogers BE, Bigott HM, McCarthy DW, Manna DD, Kim J, Sharp TL, Welch MJ: **MicroPET imaging of a gastrin-releasing peptide receptor-positive tumor in a mouse model of human prostate cancer using a** [64]**Cu-labeled bombesin analogue.** *Bioconjug Chem* 2003, **14**:756-763.

23. Thakur ML, Aruva MR, Gariepy J, Acton P, Rattan S, Prasad S, Wickstrom E, Alavi A: **PET imaging of oncogene overexpression using** [64]**Cu-vasoactve intestinal peptide (VIP) analog: comparison with** [99 m]**Tc-VIP analog.** *J Nucl Med* 2004, **45**:1381-1389.

24. Reilly RM, Sandhu J, Alvarez-Diez TM, Gallinger S, Kirsh J, Stern H: **Problems of delivery of monoclonal antibodies. Pharmaceutical and pharmacokinetic solutions.** *Clin Pharmacokinet* 1995, **28**:126-142.

25. Scollard DA, Chan C, Holloway CMB, Reilly RM: **A kit to prepare** [111]**In-DTPA-trastuzumab (Herceptin) Fab fragments injection under GMP conditions for imaging or radioimmunoguided surgery of HER-2 positive breast cancer.** *Nucl Med Biol* 2011, **38**:129-136.

26. Reilly RM: **The radiochemistry of monoclonal antibodies and peptides.** In *Monoclonal Antibody and Peptide-Targeted Radiotherapy of Cancer*. Edited by: Reilly RM. Hoboken, NJ: John Wiley 2010:39-100.

27. Orlova A, Tolmachev V, Pehrson R, Lindborg M, Tran T, Sandström M, Nilsson FY, Wennborg A, Abrahmsén L, Feldwisch J: **Synthetic affibody molecules: a novel class of affinity ligands for molecular imaging of HER2-expressing malignant tumors.** *Cancer Res* 2007, **67**:2178-2186.

28. Cheng D, Wang Y, Liu X, Pretorius PH, Liang M, Rusckowski M, Hnatowich DJ: **Comparison of** [18]**F PET and** [99 m]**Tc SPECT imaging in phantoms and in tumored mice.** *Bioconjug Chem* 2010, **21**:1565-1570.

29. Wong KJ, Baidoo KE, Nayak TK, Garmestan K, Brechbiel MW, Milenic DE: *In vitro* **and** *in vivo* **pre-clinical analysis of a F(ab'$_2$ fragment of panitumumab for molecular imaging and therapy of HER1-positive cancers.** *EJNMMI Research* 2011, **1**:1-15.

30. Boswell CA, Sun X, Niu W, Wesiman GR, Wong EH, Rheingold AL, Anderson CJ: **Comparative** *in vivo* **stability of copper-64-labeled cross-bridged and conventional tetraazamacrocyclic complexes.** *J Med Chem* 2004, **47**:1465-1474.

31. Voss SD, Smith SV, DiBartolo N, McIntosh LJ, Cyr EM, Bonab AA, Dearling JL, Carter EA, Fischman AJ, Treves ST, Gillies SD, Sargeson AM, Huston JS, Packard AB: **Positron emission tomography (PET) imaging of neuroblastoma and melanoma with** [64]**Cu-SarAr immunoconjugates.** *Proc Natl Acad Sci USA* 2007, **104**:17489-17493.